Modeling the Competition between Polymorphic Phases: Highlights on the Effect of Ostwald Ripening

Yousra Tahri, Zdeněk Kožíšek, Emilie Gagniere, Elodie Chabanon, Tijani Bounahmidi, Denis Mangin

Modeling the competition between polymorphic phases: highlights on the effect of Ostwald Ripening

Yousra Tahri*[1,2], Zdeněk Kožíšek [3], Emilie Gagnière[1],Elodie Chabanon[1], Tijani Bounahmidi[2] and Denis Mangin[1]

[1]Univ Lyon, Université Claude Bernard Lyon 1, CNRS UMR 5007, LAGEP, F-69622, Lyon, France

[2]Université Mohammed V , Ecole Mohammadia d'Ingénieurs, LASPI, Avenue Ibnsina, BP.765 RABAT-AGDAL (Morocco)

[3] Institute of Physics CAS, Cukrovarnicka 10, 16200 Praha 6, Czech Republic

Abstract: This work aims to evaluate the effect of Ostwald ripening on the crystallization of polymorphic phases by means of the kinetic equation model that was adapted to describe the competition between the nucleation, the growth and the Ostwald ripening of the different phases. The kinetic equation model is a very convenient way to simultaneously implement these three mechanisms and quantify their respective roles on the formation and the dissolution of the clusters. The polymorphic system studied is L-Glutamic acid (LGlu), which exhibits two monotropic polymorphs: α LGlu and β LGlu. The model assumptions consider the main differences between both polymorphs (shape, solubility, interfacial energy and growth rate) as well as the supersaturation decrease. The simulations results at various temperatures show that the crystallization process of small nuclei (<40nm) can be very affected by Ostwald ripening mechanism. In particular, Ostwald ripening can induce the total dissolution of the stable phase clusters, leading to a result in agreement with the Ostwald rule of stages. Thus, the numerical results suggest that the Ostwald ripening mechanism could explain the Ostwald rule of stages.

Corresponding Author

Address: Université Lyon 1 LAGEP CNRS UMR 5007, Bâtiment CPE - 308 G, 43 Boulevard du 11 Novembre 1918 69622 Villeurbanne FRANCE
Phone : (33) 472 43 18 72
Fax : (33) 472 43 16 99
E-mail : tahri@lagep.univ-lyon1.fr

Modeling the competition between polymorphic phases: highlights on the effect of Ostwald Ripening

Yousra Tahri*[1,2], Zdeněk Kožíšek [3], Emilie Gagnière[1],Elodie Chabanon[1], Tijani Bounahmidi[2] and Denis Mangin[1]

[1]Université de Lyon, Université Claude Bernard Lyon 1, CNRS, UMR 5007, LAGEP, 43 Boulevard du 11 Novembre 1918, 69622 Villeurbanne (France)

[2]Université Mohammed V , Ecole Mohammadia d'Ingénieurs, LASPI, Avenue Ibnsina, BP.765 RABAT-AGDAL (Morocco)

[3] Institute of Physic CAS, Cukrovarnicka 10, 16200 Praha 6, Czech Republic

*Corresponding author: tahri@lagep.univ-lyon1.fr

Abstract: This work aims to evaluate the effect of Ostwald ripening on the crystallization of polymorphic phases by means of the kinetic equation model that was adapted to describe the competition between the nucleation, the growth and the Ostwald ripening of the different phases. The kinetic equation model is a very convenient way to simultaneously implement these three mechanisms and quantify their respective roles on the formation and the dissolution of the clusters. The polymorphic system studied is L-Glutamic acid (LGlu), which exhibits two monotropic polymorphs: α LGlu and β LGlu. The model assumptions consider the main differences between both polymorphs (shape, solubility, interfacial energy and growth rate) as well as the supersaturation decrease. The simulations results at various temperatures show that the crystallization process of small nuclei (<40nm) can be very affected by Ostwald ripening mechanism. In particular, Ostwald ripening can induce the total dissolution of the stable phase clusters, leading to a result in agreement with the Ostwald rule of stages. Thus, the numerical results suggest that the Ostwald ripening mechanism could explain the Ostwald rule of stages.

1. Introduction:

Polymorphism denotes a substance ability to form different crystalline structures (polymorphs) characterized by different unit cells [1]. Polymorphs have the same chemical composition but different physical properties (solubility, density, crystal habit, hardness, optical properties, melting point etc.) [2] and are then considered as different materials [1]. At a given temperature and pressure, for monotropic systems, only one polymorph is thermodynamically stable, however a less stable polymorph, i.e. a metastable form, may crystallize preferentially [3]. Hence, the ability to characterize all the polymorphs, and discover the stable phase, in particular, is of crucial importance, especially with pharmaceuticals [4]. Producing a metastable phase of an active ingredient can lead to huge financial losses: the emergence of a more stable polymorph may inhibit the formation of the less stable one which was initially manufactured [5]. However, why does the metastable form crystallize first?

To explain the preferential (sometimes exclusive) crystallization of the metastable form, two reasons may be retained: first of all, the inhibition of the stable phase formation due to the solvent nature or the presence of foreign particles, acting as template [6]; secondly, the kinetic advantage of the metastable form which is expressed through the Ostwald rule of stages[7]. According to this rule, the metastable phase appears first, then undergoes a polymorphic transition toward the stable phase once this latter nucleates. Modeling the spontaneous nucleation of the metastable polymorph followed by the spontaneous nucleation of the stable polymorph using a population balance equation (PBE) is rather difficult. PBE models usually take into account nucleation, growth, agglomeration and breakage [8,9]. Such models will show the nucleation of both phases (stable and metastable) from the beginning, not only the metastable

phase. To overcome this problem, we suggest to take into account another phenomenon: the Ostwald ripening.

The Ostwald ripening is a process of particle coarsening that occurs due to the solubility difference between small and large particles: in a solution that contains particles of the same phase and of different sizes, the larger particles tend to grow at the expense of the smaller ones[10]. Ostwald ripening influences the number of remaining nuclei, since it affects particles of size lower than 1μm[11]. Vetter et al.[12] have suggested two models that took into account the Ostwald ripening in crystallization processes. The first model was based on PBE, the second one used the kinetic equations [13–15] (KE). They mentioned that PBE model is not suitable for describing nucleation and Ostwald Ripening simultaneously. On the contrary, the KE model is able to describe simultaneously nucleation, growth and Ostwald ripening [12,14]. Rempel et al. [16] used the discrete kinetic equation to describe the combined nucleation and growth of semiconductor nanocrystals. Madras et al. [17] modeled the crystallization of polymorphs by taking into account Ostwald ripening by means of "the governing population dynamics equations". The authors showed that, due to Ostwald ripening, the most stable form grew at the expense of the metastable one. Ozkan et al. [18] also considered the Ostwald ripening in Lifshitz–Slyozov, Wagner (LSW) equation in order to model the evolution of silica polymorphs through years.

Thus, until now, the effect of Ostwald ripening on the first steps of polymorph crystallization was never considered to explain the Ostwald rule of stages. At the beginning of the crystallization process, several polymorphic phases are likely to nucleate, including the stable form. However, depending on the respective growth rates of each phase, the nuclei of the polymorph of higher growth rate will then grow faster than the others and will consume the supersaturation. In the same time, the nuclei of the slow growing phases will find themselves

under the critical size and will be doomed to dissolve. Consequently, the ripening mechanism could drive the dissolution of the stable phase clusters in favor of the metastable phase, leading to the absence of stable phase crystals, in agreement with the Ostwald rule of stages. Let us note that, since this ripening mechanism does not only occur between particles of the same phase, it does not rigorously correspond to the so-called Ostwald ripening mechanism, which, in principle, concerns only crystals of one single phase. But, it is very similar to Ostwald ripening and can be assimilated to it, since it is also the consequence of the Gibbs-Thomson effect. Thus, for the sake of simplicity, we have chosen to designate this ripening mechanism by the term "Ostwald ripening" in this study although it also affects polymorphs. This work is focused on the modelling of the first steps of polymorph crystallization. For the first time, the discrete KE are used to model nucleation, growth and Ostwald ripening for a dimorphic system with taking into account supersaturation decrease [19]. The polymorphic system chosen was L-Glutamic acid (LGlu).

The cooling crystallization of LGlu polymorphs in water were already investigated [20]. This amino acid has two well-known polymorphs: a stable form β shaped as needles [21] or as lozenge slabs [20] (newly reported) and a metastable form α shaped as prisms. At the metastable zone limit, the β form was found to nucleate predominantly at 40°C, the α form nucleates predominantly at 5°C, while both polymorphic forms were observed almost evenly at 20°C [20]. The results of the KE model were compared qualitatively to these experimental data. By taking into account the Ostwald ripening, this study aimed at checking whether the KE model can reflect the competition between polymorphic phases.

2. Model

2.1. Kinetic equations:

The kinetic equations take into account nucleation, growth and Ostwald ripening [14].In the case of a polymorphic system, the kinetic equations can be expressed by [19] :

$$\frac{dF_i^{\kappa}(t)}{dt} = A_{i-1}^{\kappa} * F_{i-1}^{\kappa} - (A_i^{\kappa} + D_i^{\kappa}) * F_i^{\kappa} + D_{i+1}^{\kappa} * F_{i+1}^{\kappa} = J_{i-1}^{\kappa} - J_i^{\kappa} \quad \text{for } i > 1 \qquad (1)$$

Where:

$$J_i^{\kappa} = A_i^{\kappa} F_i^{\kappa} - D_{i+1}^{\kappa} F_{i+1}^{\kappa} \qquad (2)$$

While $\kappa=\alpha$ for the polymorph α and $\kappa=\beta$ for the polymorph β, i is the cluster size (i.e. the number of monomers forming the cluster), i goes from 2 + to M with M the maximum cluster size, $F_i^{\kappa}(t)$ is the number density of the clusters of size i, i.e. the number of nuclei formed by i monomers in unit mass at time t (kg^{-1}), A_i^{κ} and D_i^{κ} are respectively the attachment and the detachment frequencies of monomers for a cluster of size i (s^{-1}). J_i^{κ} corresponds to the rate of formation of an i-sized cluster, i.e. the number of i-sized nuclei formed per unit mass and per second ($kg^{-1}\ s^{-1}$). In standard nucleation theory, J_i^{κ} is named nucleation rate only for critical size ($i = i_c^{\kappa}$). For the sake of simplicity, the term "nucleation rate" will be abusively used to denote J_i^{κ}, whatever the size i.

2.2. Attachment and detachment frequencies:

The attachment frequency, in the case of homogeneous nucleation from solution, can be expressed as follows [13,15,22,23]:

$$A_i^{\kappa} = X_n^{\kappa} N_s^{\kappa} \left(\frac{k_B T}{h}\right) \exp\left(-\frac{E^{\kappa}}{k_B T}\right) \exp\left(-\frac{q^{\kappa}(W_{i+1}^{\kappa} - W_i^{\kappa})}{k_B T}\right) \qquad (3)$$

Where [23]:

$$\begin{cases} q^{\kappa} = 1 \quad \text{for} \quad i < i_c^{\kappa} \end{cases} \qquad (4)$$

$$q^{\kappa} = 0 \quad \text{for} \quad i \geq i_c^{\kappa}$$

X_n^{κ} is the molar fraction of LGlu in solution (-), N_s^{κ} is the number of nucleation sites on the cluster surface (-), k_B is the Boltzmann constant (J K^{-1}), T is the crystallization temperature (K), h is the Planck constant (J s), E^{κ} is the kinetic barrier of nucleation (J), and W_i^{κ} is the work of formation of an i-sized cluster (J), i_c^{κ} is the critical size. Within the capillarity approximation [14], in the case of homogeneous nucleation, the work of formation can be expressed by:

$$W_i^{\kappa} = -i * \Delta\mu^{\kappa} + \gamma^{\kappa} i^{\frac{2}{3}} \sigma^{\kappa} \quad (5)$$

Where $\Delta\mu^{\kappa}$ is the difference in chemical potential (J). For ideal solution, or real solution with reasonable supersaturation $\Delta\mu^{\kappa} = k_B T \ln(S^{\kappa})$ where S is the supersaturation ratio (-). γ^{κ} is the surface shape factor (m^2) and σ^{κ} is the interfacial energy (J m^{-2}). The critical size i_c^{κ} can be deduced from equation (5) and is given by the following equation:

$$i_c^{\kappa} = \left(\frac{2 * \gamma^{\kappa} \sigma^{\kappa}}{3 \Delta\mu^{\kappa}}\right)^3 \quad (6)$$

The detachment frequency is usually determined from the principle of local thermodynamic equilibrium [15]. This method is one of the indirect methods that determines detachment frequency using attachment frequency (see section 10.2 in reference [14]) and was originally introduced by Zeldovich [24]. The idea behind is that when the system is in thermodynamic equilibrium, the equilibrium is maintained by the detailed balance (i.e. the balance holding at any cluster size i) between the number of attachments to all i-sized clusters in the system and the number of detachments from all (i+1)-sized clusters in it. The cluster population, which is needed kinetically to ensure this microscopic reversibility or detailed balance, is represented by the equilibrium cluster size distribution. Thus, the condition for this reversibility is given by [14,15,24]:

$$A_i^{\kappa} F_i^{\kappa,0} = D_{i+1}^{\kappa} F_{i+1}^{\kappa,0} \quad (7)$$

Where $F_i^{\kappa,0}$ is the equilibrium number density of clusters of size i, within context of self-consistent model, $F_i^{\kappa,0}$ can be written [25] as:

$$F_i^{\kappa,0} = N_1 \exp\left(\frac{W_1^{\kappa}}{k_B T}\right) \exp\left(-\frac{W_i^{\kappa}}{k_B T}\right) \quad (8)$$

Where N_1 is the initial number of monomers within the liquid phase (kg^{-1}) and does not depend on the polymorphic phases.

It is worth noting that the exact formula for the stationary nucleation rate (at constant temperature and supersaturation) is [14]:

$$J_s^{\kappa} = \left(\sum_{i=1}^{M} \frac{1}{A_i^{\kappa} F_i^{\kappa,0}}\right)^{-1} \quad (9)$$

The stationary nucleation rate is an upper limit for the nucleation rate for any cluster size i, because it corresponds to the rate of cluster formation in the case of constant supersaturation and temperature (open system). This rate is introduced just for comparison.

2.3. Boundary conditions:

The standard model of nucleation does not take into account the supersaturation decrease, i.e the number of monomers within the system does not change. However, in closed system, the number of monomers in the liquid phase decreases and the assumption of a constant supersaturation is no longer valid. In this latter case, and for the polymorphic system studied, the following initial and boundary conditions were used:

$$F_i^{\kappa}(t = 0) = F_i^{\kappa,0}, \text{ for } i \leq i_0 \quad (10)$$

$$F_i^{\kappa}(t = 0) = 0, \text{ for } i > i_0 \quad (11)$$

$$F_1^{\kappa}(t) = N_T^{\kappa} - \left(\sum_{i>1} i F_i^{\alpha}(t) + \sum_{i>1} i F_i^{\beta}(t)\right), \ \forall t \quad (12)$$

$$F_M^{\kappa}(t) = 0, \ \forall t \quad (13)$$

At the initial time, the size distribution was taken equal to the equilibrium distribution up to the cluster size $i_0 = 10$. This assumption takes into account the preexistence, in the suspension, of subcritical cluster formed of two monomers up to ten monomers. The equilibrium size distribution for small cluster sizes is a good approximation of the number of subcritical clusters formed due to fluctuation within system. In classical nucleation theory i_0=1 and decrease of monomers is not taken into account. Kožíšek and Demo [26] showed that the assumption i_0=1 (only monomers are present within solution) leads in closed systems to fast decrease in supersaturation, which does not fit with experimental data. With increasing value of i_0, this effect decreased. It was recommended to take $5 < i_0 < i_c/2$. Accordingly, i_0 was taken equal to ten in this study because this value obeys to these conditions within the range of temperature and supersaturation considered. N_T^K is the total number of LGlu monomers in the system (even those forming the crystals) :

$$N_T^K = N_1 + \left(\sum_{i=2}^{i_0} i\, F_i^{\alpha,0}(t=0) + \sum_{i=2}^{i_0} i\, F_i^{\beta,0}(t=0)\right) \qquad (14)$$

N_T^K does not vary with time.

2.4. Main differences between α and β LGlu:

2.4.1. Shape:

Both α LGlu and β LGlu have the same orthorhombic space group $P2_12_12_1$ but the cell constants are different [27] (see Table 1).

Table 1 : Unit cell constants for α and β LGlu

	α form	**β form**
a_0 (Å)	7.068	5.519
b_0 (Å)	10.277	17.30
c_0 (Å)	8.755	6.948

It was assumed that the crystals of both polymorphs will keep the same shape as their unit cell (see Figure.1) according to the following equation:

$$\frac{a}{a_0} = \frac{b}{b_0} = \frac{c}{c_0} \tag{15}$$

Where a,b,c are the crystal dimensions (see Figure 1).

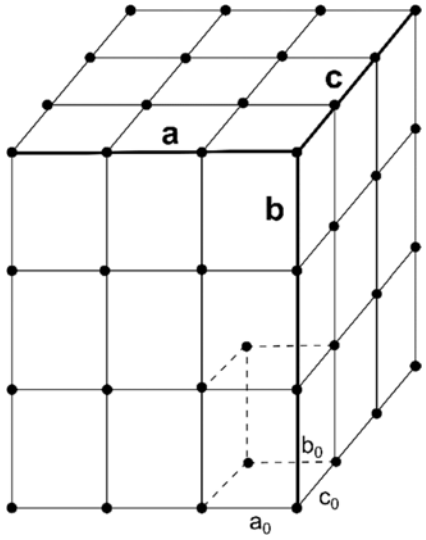

Figure 1 : Crystal dimensions vs unit cell dimension for both LGlu polymorphs

The characteristic size r of α and β crystals was taken equal to the larger length b. According to this assumption, r can be related to the number of monomers forming the clusters as follows:

$$r = \left(\frac{m_1}{v_0^\kappa \rho^\kappa}\right)^{\frac{1}{3}} b_0^\kappa \, i^{1/3} = \varphi^\kappa \, i^{1/3} \tag{16}$$

The surface shape factor introduced earlier in the equation (5) can be deduced:

$$\gamma^\kappa = 2\left(\frac{a_0^\kappa}{b_0^\kappa} + \frac{a_0^\kappa \, c_0^\kappa}{(b_0^\kappa)^2} + \frac{c_0^\kappa}{b_0^\kappa}\right)\left(\left(\frac{m_1}{v_0^\kappa \rho^\kappa}\right)^{\frac{1}{3}} b_0^\kappa\right)^2 \tag{17}$$

Where v_0^κ is the unit cell volume (m^3), m_1 is the monomer mass (kg) and $\rho^\kappa$is the crystal density (kg m^{-3}).

It is to note that, from shape assumption, it is possible to define the number of nucleation sites on the cluster surface (see equation (3)) as:

$$N_S^{\kappa} = 6 * \left(\frac{r^{\kappa}}{b_0^{\kappa}}\right)^2 + 2 \quad (18)$$

The equation (18) derivation is explained in the Appendix A in the supporting information.

2.4.2. Solubility:

Solubility data of both polymorphs have been determined previously [20]. The dependence of the equilibrium molar fraction on the temperature is given by:

$$ln(X_e^{\alpha}) = -\frac{3485.7}{T} + 5.10 \quad (19)$$

$$ln\left(X_e^{\beta}\right) = -\frac{3494.4}{T} + 4.85 \quad (20)$$

2.4.3. Interfacial energy:

The interfacial energy is a very important parameter in our computations and the values that can be deduced from literature can be very different from one reference to the other (see section below). As a first step, we thus tried to estimate an upper limit for the interfacial energy of both polymorphs.

Evaluating the maximum interfacial energy:

The maximum threshold of the interfacial energy of each polymorph is the value that allows simulating the nucleation of at least one nucleus per cm^3 of solvent (i.e. 1000 nuclei per kg of solvent). One nucleus per cubic centimeter corresponds to the nucleation detection limit according to the work of Boistelle and Astier [11]. Below this limit, nucleation can be considered negligible. Thus, the stationary number density of nuclei (the stationary number density is an upper limit for the number density) should be:

$$F_{ic}^{\kappa,s} = 1000\ (kg^{-1})$$

This stationary number density can be approximated (see equation 13.23 in reference [14]) by:

$$F_{i_c}^{\kappa,s} = \frac{1}{2} F_{i_c}^{\kappa,0} \tag{21}$$

Where $F_{i_c}^{\kappa,0}$ is the equilibrium number density at the critical size i_c (kg^{-1}). Thus, the maximum value of interfacial energy can be deduced from the following equation:

$$\frac{1}{2} F_{i_c}^{\kappa,0} = 1000 \tag{22}$$

That leads to (for more details, see Appendix B in the supporting information):

$$\frac{\gamma^{\kappa}\sigma_{max}^{\kappa}}{k_B T}\left(\frac{24}{7}\frac{(\gamma^{\kappa}\sigma_{max}^{\kappa})^2}{(k_B \mathrm{T})^2}\frac{1}{ln^2\, S^{\kappa}} - 1\right) + ln\left(\frac{2000}{N_a C_e^{\kappa}(T)}\right) = 0 \tag{23}$$

Where $C_e^{\kappa}(T)$ denotes the solubility of the polymorph κ (mol kg^{-1} of solvent).

Thereby, the maximum value of the interfacial energy, at the temperature T and the supersaturation S, can be deduced by solving equation (23).

At the temperatures T=5, 20 and 40°C , the maximum supersaturation ratios that can be reached are respectively 4.22, 3.18 and 2.05, according to the α solubility and 5.59, 4.21 and 2.71 according to the β solubility (these supersaturations correspond to the metastable zone limit in the case of cooling crystallization with a quick cooling rate [20]).

In order to avoid a very high nucleation barrier, the maximum values of interfacial energy for α and β, at T=5, 20 and 40°C and at the corresponding maximum supersaturations, are shown in Table 2.

Table 2: Maximum values of interfacial energy at different temperatures and supersaturations

Temperature (°C)	**Supersaturation ratio according to α solubility (-)**	**Supersaturation ratio according to β solubility (-)**	**maximum value of interfacial energy for α (J/m^2)**	**maximum value of interfacial energy for β (J/m^2)**
5	4.22	5.59	0.0194	0.0205
20	3.18	4.21	0.0176	0.0191
40	2.05	2.71	0.0136	0.0159

Comparing the interfacial energies of α and β deduced from litterature and selecting the values for the computations:

According to the work of Deij et al. [28], at 20°C and for the crystal shape used in this study, the interfacial energies for α and β are respectively 0.023 and 0.020 ($J\ m^{-2}$)

The interfacial energy can also be deduced from the nucleation data [29]. The homogeneous nucleation rate can be expressed as:

$$J = A_{hom} * exp\ (-\frac{B_{hom}}{ln^2(S)}) \quad (24)$$

With:

$$B_{hom} = \frac{4}{27} * \left(\frac{\sigma\ \gamma}{k_b T}\right)^3 \quad (25)$$

Lindenberg et al. [30] determined nucleation kinetics of α LGlu at different temperatures using the induction time method. Then, it is possible to deduce the interfacial energy from the kinetic law they established with their experimental data. It is worth noting that we used the data at the high supersaturation regime [30], because they are more likely to correspond to homogeneous nucleation. It is also important to note that Lindeberg et al. made the assumption of spherical crystals.

Another way to determine the interfacial energy is to use the solubility data. Mersmann [31] proposed the following equation, relating the interfacial energy to the solubility:

$$\sigma = 0.414 * k_b\, T\, \left(\frac{\rho N_a}{M_n}\right)^{\frac{2}{3}} * ln\left(\frac{\rho}{M_n * C_e(T)}\right) \quad (26)$$

Where N_a is Avogadro number (mol^{-1}), M_n is the molar mass and $C_e(T)$ is the solubility at the temperature T.

Bennema et al. [32] also related the interfacial energy to the solubility as follows:

$$\sigma = k_b\, T\, \left(V_m^{-\frac{2}{3}}\right) * 0.25 * (0.7 - ln(X_e)) \quad (27)$$

Where V_m is the molecular volume (m^3) and X_e is the solubility expressed in molar fraction (-).

By choosing suitable standard states at the solubility equilibrium, Christoffersen et al. [33] suggested the following expression for the interfacial energy:

$$\sigma = \frac{k_b\, T}{\pi\, d^2}\, ln\left(\frac{C_x}{C_e(T)}\right) \quad (28)$$

with $C_x = \frac{\rho}{M_n}$ and d is the molecular diameter.

The values of interfacial energy calculated from the above equations for each LGlu polymorph along with the maximum value taken from table 2 are shown in Figure 2-a and Figure 2-b. From these results, it can be deduced that the interfacial energy of α is lower than that of β. This is linked to their solubility values. Also, it seems reasonable to take the following interfacial energies all over the studied temperature range (see Figure 2-a and 2-b):

$$\sigma^{\alpha} = 0.013\ \ (J\, m^{-2})$$

$$\sigma^{\beta} = 0.014\ \ (J\, m^{-2})$$

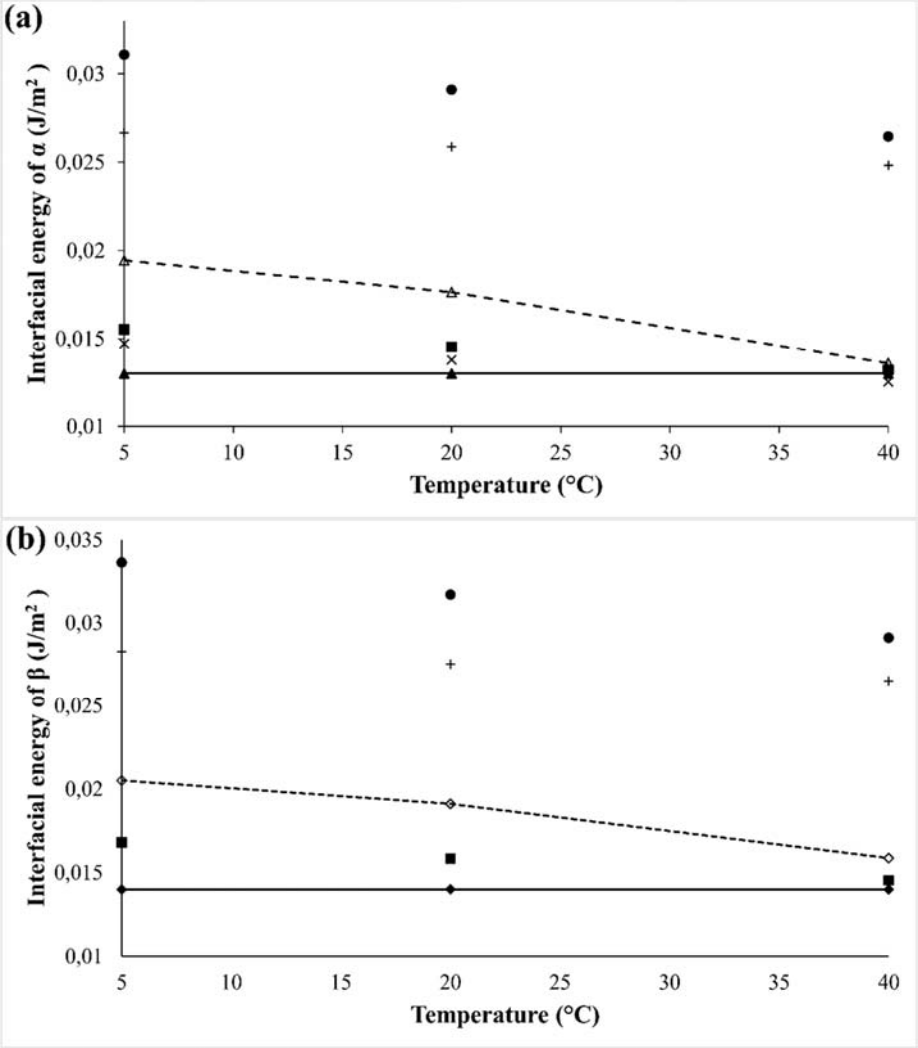

Figure 2: Estimations of interfacial energy of α and β LGlu at different temperatures: (a) α phase (b) β phase. ● Mersmann [31], + Bennema et al. [32], ■ Christoffersen [33] x Lindenberg et al. [30]. Dashed line shows the maximum interfacial energy (see Table 2). Solid line corresponds to the interfacial energy in this work.

2.4.4. The kinetic barrier of nucleation

In the case study, since the growth rate of LGlu polymorphs is known to be controlled by surface integration [34], the kinetic barrier of nucleation E mentioned in equation (3) is the

activation energy for interface transfer [14]. The term $exp\left(-\frac{E^{\kappa}}{k_B T}\right)$ can be deduced from the growth rate.

The growth rate ϑ^{κ} of a nucleus [35] is given by:

$$\vartheta^{\kappa}(i) = \frac{dr}{dt} = \frac{dr}{di} * \frac{di}{dt} \tag{29}$$

Where $\frac{di}{dt}$ can be determined in terms of attachment and detachment frequencies:

$$\frac{di}{dt} = A_i^{\kappa} - D_{i+1}^{\kappa} = A_i^{\kappa}\left[1 - \frac{F_i^{\kappa,0}}{F_{i+1}^{\kappa,0}}\right] \tag{30}$$

The growth rate at the limit $i \to \infty$ can be written as:

$$\vartheta^{\kappa}(i \to \infty) = G^{\kappa} = \ 2 * X_n^{\kappa} * (\frac{m_1\, b_0^{\kappa}}{v_0^{\kappa} * \rho^{\kappa}}) * \left(\frac{k_B T}{h}\right) exp\left(-\frac{E^{\kappa}}{k_B T}\right) * \left(\frac{S^{\kappa}-1}{S^{\kappa}}\right) \tag{31}$$

The activation energy can be deduced from the growth rate since all the parameters in equation (28) are known. The growth rates of α and β correspond to birth and spread mechanisms [34] and were taken from Schöll et al [36] and Ochsenbein et al. [37] works, respectively:

$$G^{\alpha}(T,S) = 3.50 * 10^{-4}\, T\ exp\left(-\frac{3.72*10^3}{T}\right)\ (S^{\alpha}-1)^{\frac{2}{3}}\ (ln\, S^{\alpha})^{\frac{1}{6}}\ exp\ (-\frac{5.42*10^4}{T^2\ lnS^{\alpha}}) \tag{32}$$

$$G^{\beta}(T,S) = 4.23 * 10^{-4}\ exp\left(-\frac{2.62*10^3}{T}\right)\ \left(S^{\beta}-1\right)^{\frac{2}{3}}\left(ln\, S^{\beta}\right)^{\frac{1}{6}} exp\ (-\frac{5*10^4}{T^2\ lnS^{\beta}}) \tag{33}$$

It is worth noting that the growth rate of α LGlu was multiplied by a corrective factor (see equation (27) in Schöll et al. article [36]) to satisfy the shape assumption done in this work. Also, the β growth rate parameters were tuned to approach (for a supersaturation ratio S=2) the data given by Cornel et al. [38] at 45°C and to correspond to the data given by Kitamura et al. [34] at 25°C. It is also to note that the growth rate of α is several times higher than that of β at all temperatures.

3. Results and discussion:

Crystallization of both polymorphs of L-Glutamic acid at constant temperature was considered. For the sake of simplicity, only homogeneous nucleation was taken into account. The model parameters were fixed as follows: crystal density of α $\rho^{\alpha} = 1533\, kg\, m^{-3}$, crystal density of β $\rho^{\beta} = 1590\, kg\, m^{-3}$. The kinetic equations were solved up to the size of 300 000 monomers for the α form (equivalent to a characteristic size of 43.4 nm) and up to 20 000 monomers for the β form (equivalent to a characteristic size of 28.8 nm) ($M^{\alpha} = 300\,000$; $M^{\beta} = 20\,000$). It is to note that the difference between the maximum sizes of α and β are due to the shape assumptions made in section 2.4.1. The initial conditions are summarized in Table 3.

Table.3: Initial conditions of the model

Temperature (°C)	**initial concentration (mol/kg of solvent)**	**Supersaturation ratio according to α solubility (-)**	**Supersaturation ratio according to β solubility (-)**
5	0.139	4.22	5.59
20	0.199	3.18	4.21
40	0.274	2.05	2.71

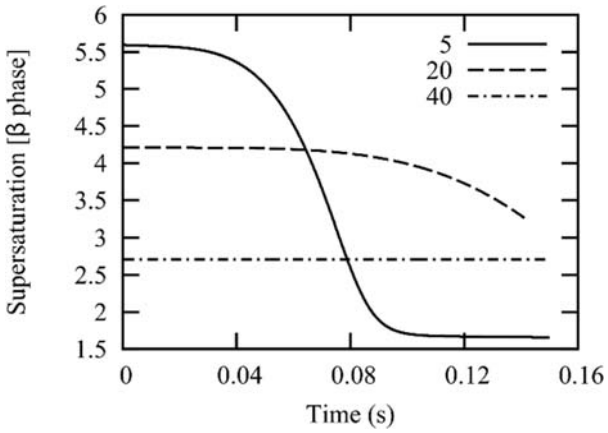

Figure 3: Evolutions of the supersaturation (according to the β solubility) with time at 5, 20 and 40°C

The evolution of the supersaturation ratio (according to β solubility) with time at different temperatures is depicted in Figure 3. It is worth noting that the supersaturation ratio is only related to the number of monomers within the solution ($S=F_1/N_e$ with N_e the number of monomers at the equilibrium concentration). At 40°C, the supersaturation decrease is negligible because the initial energy barrier of nucleation for both phases is high ($W_{i_c}^{\alpha}/(K_B\,T) = 44.5$ and $W_{i_c}^{\beta}/(K_B\,T) = 35.65$). This is due to the low initial supersaturation chosen. At 20°C and 5°C, since the initial supersaturations were high (see Table 3), the initial energy barrier of nucleation was found to be low for both phases (at 20°C: $W_{i_c}^{\alpha}/(K_B\,T) = 20.88$, $W_{i_c}^{\beta}/(K_B\,T) = 20.90$ and at 5°C: $W_{i_c}^{\alpha}/(K_B\,T) = 15.78$ and $W_{i_c}^{\beta}/(K_B\,T) = 17.07$) and the monomers within the solution started quickly to be consumed by the crystallization process. The energy barrier of nucleation is influenced by two parameters: supersaturation and interfacial energy. At 40°C the difference in solubility between α and β is significant and gives the advantage to the β phase, so β nucleation has a lower energy barrier at this temperature. Conversely, at 5°C the solubility of α and β are very close, inducing very close supersaturations. The difference in energy barrier calculation comes then from the interfacial energies. In that case, α nucleation has the lowest energy barrier (see Tahri et al. article [20] for α and β solubility curves).

The supersaturation depletion at 20°C caused an increase with time in the energy barrier of nucleation of α and β as shown in Figure 4. For the sake of simplicity, the results at 5°C and 40°C were not added: at 5°C, similar behavior as that obtained at 20°C is observed, while at

40°C the initial work of formation of both phases remained constant with time due to constant supersaturation

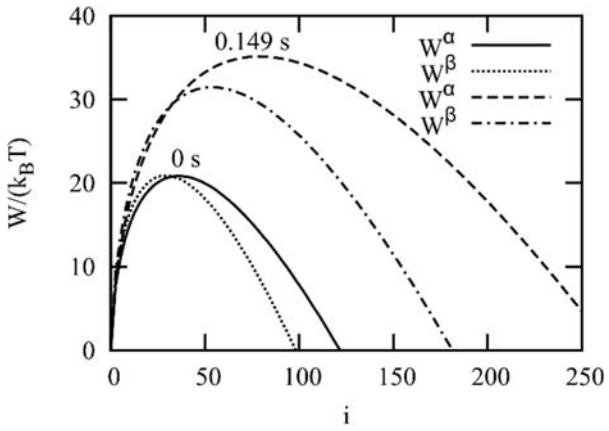

Figure 4: Dimensionless work of formation of α and β clusters as a function of size at various times and at 20°C

At 5°C, the supersaturation decrease was very important. As a consequence the critical size of both α and β nuclei increased significantly with time: i_c evolved from 22 monomers (equivalent to 1.8 nm) for α and 20 (equivalent to 2.9 nm) for β to more than 5000 for α (equivalent to 11.1 nm) and more than 700 for β (equivalent to 9.4 nm) (see Figure 5). At 20°C, the critical size of both polymorphs slightly increased. Obviously, it remained constant with time at 40°C (see Figure 5).

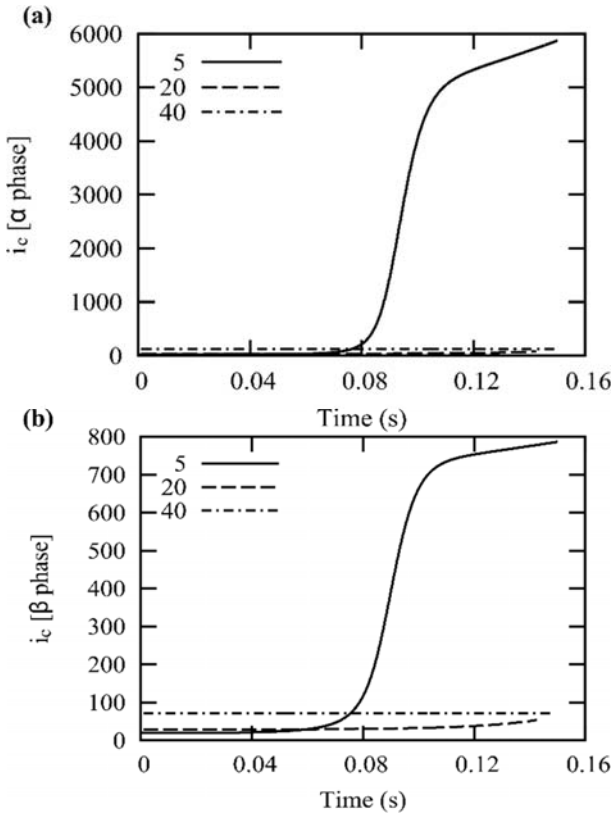

Figure 5: The critical size ic of α and β phases as a function of time at 5, 20 and 40°C: (a) α phase (b) β phase

The cluster size distribution at different times at 5°C are shown in Figure 6. The first thing to notice in this figure is the vanishing of the β nuclei with time: at 0.05s the number of supercritical clusters is more than 10^{15} per unit mass of suspension (critical size is about 2.9 nm at that time), while the number of supercritical clusters is zero at 0.95s (critical size is higher than 9.4nm at that time) (Figure 6-b). Even, the α phase nuclei slightly dissolve (Figure 6-a). The important dissolution of the β nuclei at 5°C is caused by "Ostwald ripening", i.e. Gibbs-Thomson effect. At the beginning, when the supersaturation of both phases was high, α and β nucleated significantly. However, since the α phase nuclei grew several times faster than the β phase and consumed the supersaturation, the β nuclei became quickly smaller than the critical size and

dissolved. In addition to that, dissolution also affected some of α nuclei: when the supersaturation dropped, the α crystals that had nucleated earlier were large enough and kept on growing and consuming supersaturation, while the youngest α crystals became smaller than the critical size and dissolved. That latter case corresponds rigorously to the so called Ostwald ripening.

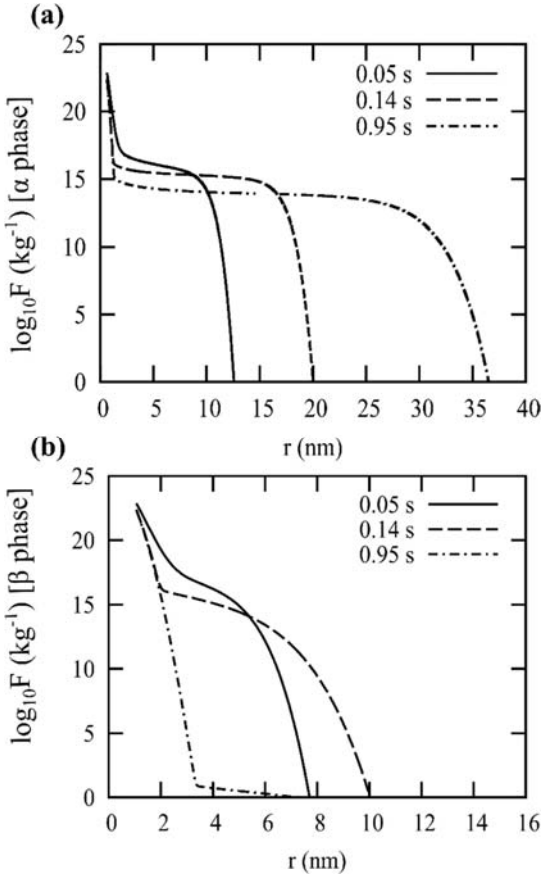

Figure 6: The cluster size distribution of α and β at 5°C at various times: (a) α phase (b) β phase

In Figure 7, the nucleation rate J of each polymorph is scaled by the initial value of the stationary nucleation rate, $J_s^{\kappa}(t=0)$, computed from equation (3). At 5°C, the nucleation rate of both phases for a size i=200 (supercritical at initial time) reached a maximum value then became negative. This result, that can seems rather surprising, is due to the supersaturation decrease and

the rise of the critical size; at t≈0.08s, the 200-sized clusters became subcritical, so their attachment frequency fell below their detachment frequency and thus, the nucleation rate became negative. These results confirmed our previous observations about clusters dissolution at 5°C. At 20°C, the nucleation rate of α and β reached a maximum value then decreased due to supersaturation depletion. At 40°C, since the supersaturation remained constant, the system behave as an open system that follows the standard model of nucleation [19]. It is worth noting that the dimensionless nucleation rate was depicted for i=200 just as an example, because this size is a supercritical size at all the initial conditions and it clearly allows showing the trends at all the studied temperatures.

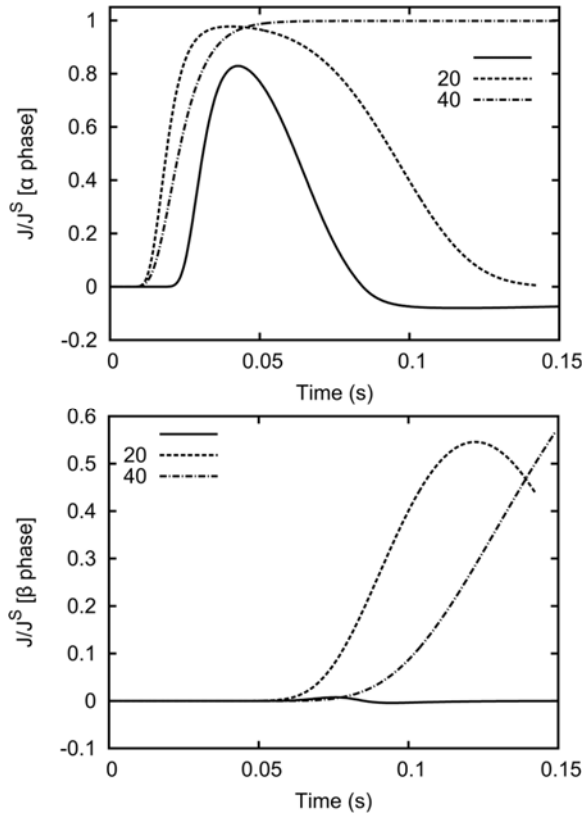

Figure 7: Dimensionless nucleation rate as a function of time at 5, 20 and 40°C for a size i=200:

(a) α phase (b) β phase

To compare qualitatively our numerical results to experimental data, the following crystallization fractions of α and β forms were introduced:

$$X^{\alpha} = \frac{\sum_{i=2}^{M^{\alpha}} i\, F_i^{\alpha}}{N_T^{\alpha}} \tag{34}$$

$$X^{\beta} = \frac{\sum_{i=2}^{M^{\beta}} i\, F_i^{\beta}}{N_T^{\beta}} \tag{35}$$

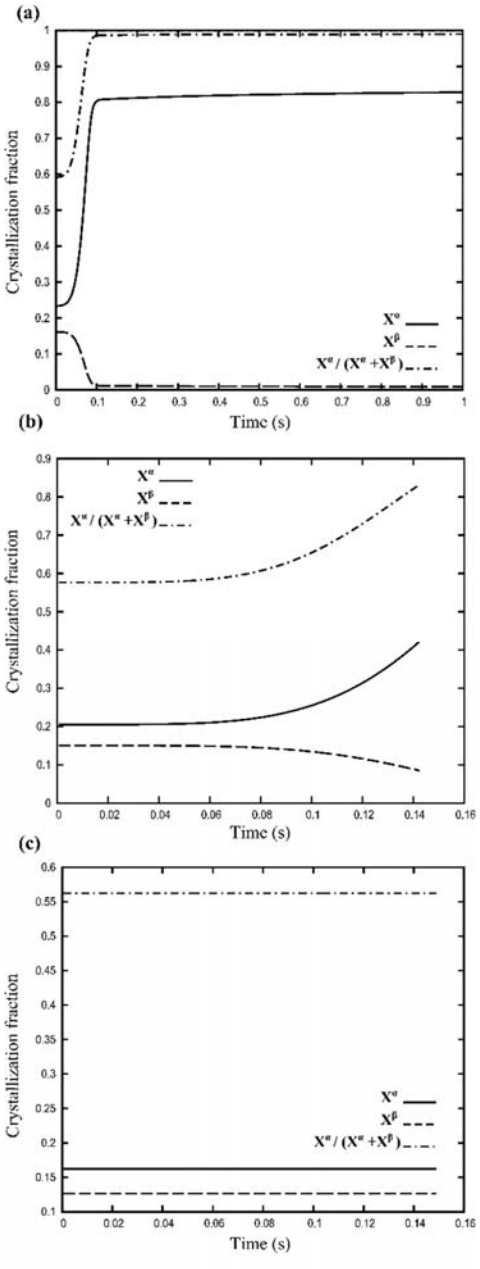

Figure 8: The crystallization fraction of α and β phases as a function of time at different temperatures: (a) 5°C, (b) 20 °C ,(C)40°C

The evolution of the crystallization of both forms at 5, 20 and 40°C is shown in Figure 8. At 5°C, the crystallization fraction of β fell down near zero because of the competition between the two polymorphs and the Gibbs-Thomson effect. It is to note that this fraction is not null because it takes into account subcritical clusters. At 20°C, the "Ostwald ripening" also affected the crystallization fraction of β but did not cause the total dissolution of this phase. At 40°C, the crystallization fractions of both polymorphs are constant with a slight advantage of α phase.

These results are compared to experimental observations in Table 4. This table shows that the numerical results show trends that are rather in good agreement with the experimental data.

Table.4: Experimental and numerical observations at various supersaturations and temperatures

Temperature (°C)	**Supersaturation ratio according to β solubility (-)**	**polymorphic phase observed in the experiments** [20]	**polymorphic phase observed in the simulations**
5	5.59	mostly α	only α
20	4.21	α and β	α and β
40	2.71	mostly β with α	α and β

Conclusion:

The influence of the Ostwald ripening on the crystallization of L-Glutamic acid polymorphs was considered using the kinetic equation (KE) model. In order to reflect experimental data, the parameters of KE model were adjusted to take into account the main differences between α LGlu and β LGlu: shape, solubility, interfacial energy and growth rate. The simulations were done at 5, 20 and 40°C. At the first moments of the crystallization process, the numerical results showed

that the α and β clusters smaller than 40nm were affected by ripening at 5°C. The ripening had a strong effect on the β phase nuclei and caused their total dissolution at 5°C. This result is in conformity with the Ostwald rule of stages. It was also found that, the competition between α and β phases was more affected by ripening mechanism at 5°C compared to 20 and 40°C. The simulations results at 5, 20 and 40°C and experimental observations were then compared qualitatively and were found to be in a good agreement. Accordingly, this work showed that the kinetic equations could be a very convenient way to model the competition between polymorphic phases and suggested that the Ostwald rule of stages could be explained by the Ostwald ripening mechanism.

Funding Sources

This work was supported by a STSM Grant from COST Action CM1402 Crystallize and by the Grant no. LD1504 (VES 15 COST CZ) from the Ministry of Education of the Czech Republic.

Acknowledgment:

The authors acknowledge gratefully The COST Action CM1402 and The Ministry of Education of the Czech Republic for funding.

Supporting information:

Derivation of equation (18), demonstration of equation (23) from equation (22).

Symbols:

A_i: Attachment frequency of monomers for a cluster of size i (s^{-1}).

A_{hom}: Pre-exponential factor in the general expression of homogeneous nucleation rate ($kg^{-1}\ s^{-1}$).

a, b, c : Crystal dimensions (m^{-3})

a_0, b_0, c_0: Unit cell constants (Å)

B_{hom}: Exponential factor in the general expression of homogeneous nucleation rate (-)

C_e: Equilibrium concentration (mol kg^{-1} of solvent).

D_i: Detachment frequency of monomers for a cluster of size i (s^{-1})

d: Molecular diameter (m^{-3})

E: Kinetic barrier of nucleation (J)

F_i : Number density of the clusters of size i, i.e. Number of nuclei formed by i monomers (kg^{-1}).

F_i^0: Equilibrium number density of clusters of size i (kg^{-1}).

G: Size independent growth rate ($m\ s^{-1}$)

h: Planck constant (J s).

i: Cluster size, i.e. number of monomers forming the cluster (-)

i_c: Critical size (-)

i_0: determines initial size distribution of clusters (-)

J_i: Nucleation rate, i.e. the number of i-sized nuclei formed in unit mass per second ($kg^{-1}s^{-1}$)

J_s: Stationary nucleation rate ($kg^{-1}s^{-1}$)

k_B: Boltzmann constant ($J\ K^{-1}$)

M: Maximum cluster size (-)

M_n: Molar mass (kg mol^{-1})

m_1: Monomer mass (kg)

N_a: Avogadro number (mol^{-1})

N_e: Number of monomers at the equilibrium concentration (-)

N_s: Number of nucleation sites on the cluster surface (-)

N_T: Total number of LGlu monomers in the system (kg^{-1})

N_1: Initial number of monomers within the liquid is phase (kg^{-1})

r: Characteristic size of the clusters (m)

S: Supersaturation ratio (-)

T: Temperature (K)

V_m: Molecular volume (m^3)

v_0: Volume of the unit cell (m^3)

W_i: Work of formation of an i-sized cluster (J)

X_e: Equilibrium molar fraction (-).

X_n: Molar fraction of LGlu in solution (-)

γ: Surface shape factor (m^2)

$\Delta\mu$: The difference in chemical potential (J)

ϑ: Size dependent growth rate (m s^{-1})

κ: Index that refers to α of β polymorph. $\kappa=\alpha$ for the polymorph α and $\kappa=\beta$ for the polymorph β

σ: Interfacial energy (J m^{-2}).

ρ: Crystal density (kg m^{-3}).

Bibliography

(1) Brittain, H. G. *Polymorphism in pharmaceutical solids*; Informa Healthcare: New York, 2009.
(2) Mangin, D.; Puel, F.; Veesler, S. *Org. Process Res. Dev.* **2009**, *13* (6), 1241–1253.
(3) Caira, M. R. In *Design of Organic Solids*; Weber, P. D. E., Aoyama, Y., Caira, M. R., Desiraju, G. R., Glusker, J. P., Hamilton, A. D., Meléndez, R. E., Nangia, A., Eds.; Topics in Current Chemistry; Springer Berlin Heidelberg, 1998; pp 163–208.
(4) Boukerche, M.; Mangin, D.; Klein, J. P.; Monnier, O.; Hoff, C. *Chem. Eng. Res. Des.* **2010**, *88* (11), 1474–1478.
(5) Dunitz, J. D.; Bernstein, J. *Acc. Chem. Res.* **1995**, *28* (4), 193–200.
(6) Blagden, N.; Davey, R. J. *Cryst. Growth Des.* **2003**, *3* (6), 873–885.
(7) Nývlt, J. *Cryst. Res. Technol.* **1995**, *30* (4), 443–449.
(8) Costa, C. B. B.; Maciel, M. R. W.; Filho, R. M. *Comput. Chem. Eng.* **2007**, *31* (3), 206–218.
(9) Nallet, V.; Mangin, D.; Klein, J. P. *Comput. Chem. Eng.* **1998**, *22*, S649–S652.
(10) Mullin, J. W. *Crystallization*; Butterworth-Heinemann: Oxford; Boston, 2001.
(11) Boistelle, R.; Astier, J. P. *J. Cryst. Growth* **1988**, *90* (1), 14–30.
(12) Vetter, T.; Iggland, M.; Ochsenbein, D. R.; Hänseler, F. S.; Mazzotti, M. *Cryst. Growth Des.* **2013**, *13* (11), 4890–4905.
(13) Turnbull, D.; Fisher, J. C. *J. Chem. Phys.* **1949**, *17* (1), 71–73.
(14) Kashchiev, D. *Nucleation basic theory with applications*; Butterworth Heinemann: Oxford; Boston, 2000.
(15) Kožíšek, Z.; Demo, P.; Sveshnikov, A. In *Thermal analysis of Micro, Nano- and Non-Crystalline Materials*; Šesták, J., Šimon, P., Eds.; Hot Topics in Thermal Analysis and Calorimetry; Springer Netherlands, 2013; pp 195–208.
(16) Rempel, J. Y.; Bawendi, M. G.; Jensen, K. F. *J. Am. Chem. Soc.* **2009**, *131* (12), 4479–4489.
(17) Madras, G.; McCoy, B. J. *Cryst. Growth Des.* **2003**, *3* (6), 981–990.
(18) Ozkan, G.; Ortoleva, P. *J. Chem. Phys.* **2000**, *112* (23), 10510–10525.
(19) Kožíšek, Z. *CrystEngComm* **2013**, *15* (12), 2269.
(20) Tahri, Y.; Gagnière, E.; Chabanon, E.; Bounahmidi, T.; Mangin, D. *J. Cryst. Growth* **2016**, *435*, 98–104.
(21) Kitamura, M. *J. Cryst. Growth* **1989**, *96* (3), 541–546.
(22) Kelton, K. F.; Greer, A. L. *Phys. Rev. B* **1988**, *38* (14), 10089–10092.
(23) Ziabicki, A.; Jarecki, L. *J. Chem. Phys.* **1984**, *80* (11), 5751–5753.
(24) Zeldovich, Y. B. *Acta Physicochim URSS* **1943**, *18* (1), 1–22.
(25) Courtney, W. G. *J. Chem. Phys.* **1961**, *35* (6), 2249–2250.
(26) Kožíšek, Z.; Demo, P. *J. Chem. Phys.* **2005**, *123* (14), 144502.

(27) Bernstein, J. *Polymorphism in molecular crystals*; Clarendon Press ; Oxford University Press: Oxford [England]; New York, 2002.
(28) Deij, M. A.; ter Horst, J. H.; Meekes, H.; Jansens, P.; Vlieg, E. *J. Phys. Chem. B* **2007**, *111* (7), 1523–1530.
(29) Wu, W.; Nancollas, G. H. *Adv. Colloid Interface Sci.* **1999**, *79* (2–3), 229–279.
(30) Lindenberg, C.; Mazzotti, M. *J. Cryst. Growth* **2009**, *311* (4), 1178–1184.
(31) Mersmann, A. *J. Cryst. Growth* **1990**, *102* (4), 841–847.
(32) Bennema, P.; Söhnel, O. *J. Cryst. Growth* **1990**, *102* (3), 547–556.
(33) Christoffersen, J.; Rostrup, E.; Christoffersen, M. R. *J. Cryst. Growth* **1991**, *113* (3–4), 599–605.
(34) Kitamura, M.; Ishizu, T. *J. Cryst. Growth* **2000**, *209* (1), 138–145.
(35) Kožíšek, Z.; Demo, P. *J. Aerosol Sci.* **2009**, *40* (1), 44–54.
(36) Schöll, J.; Lindenberg, C.; Vicum, L.; Brozio, J.; Mazzotti, M. *Faraday Discuss.* **2007**, *136*, 247.
(37) Ochsenbein, D. R.; Schorsch, S.; Vetter, T.; Mazzotti, M.; Morari, M. *Ind. Eng. Chem. Res.* **2014**, *53* (22), 9136–9148.
(38) Cornel, J.; Lindenberg, C.; Mazzotti, M. *Cryst. Growth Des.* **2008**, *9* (1), 243–252.

Table of Contents Graphic and Synopsis:

This paper investigates the effect of the Ostwald Ripening on the competition between polymorphic phases using a kinetic model. Numerical results and experimental data, at various temperatures, were compared qualitatively and were found to be in good agreement. The results emphasized the importance of considering the ripening mechanism when modelling polymorph crystallization.

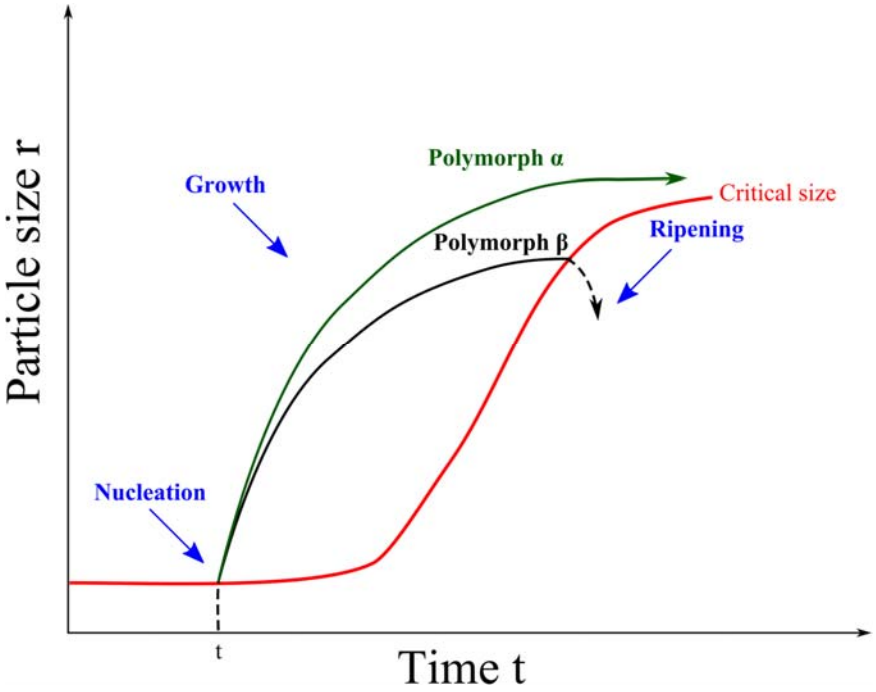
Particle size r
Growth
Polymorph α
Critical size
Ripening
Polymorph β
Nucleation
t
Time t